Evaporative Cooling via Jumping Droplet Condensation on Superhydrophobic Surfaces for Localized Car Air Conditioning

by

John Queeney

Submitted to the
Department of Mechanical Engineering
in Partial Fulfillment Requirements for the Degree of

Bachelor of Science in Mechanical Engineering

at the

Massachusetts Institute of Technology

June 2015

Signature of Author: Signature redacted

Department of Mechanical Engineering
May 19, 2015

Certified by: Signature redacted

Evelyn N. Wang
Associate Professor of Mechanical Engineering
Thesis Supervisor

Accepted by: Signature redacted

Anette Hosoi
Professor of Mechanical Engineering
Undergraduate Officer

Evaporative Cooling via Jumping Droplet Condensation on Superhydrophobic Surfaces for Localized Car Air Conditioning

by

John Queeney

Submitted to the Department of Mechanical Engineering
on May 19, 2015 in Partial Fulfillment of the
Requirements for the Degree of

Bachelor of Science in Mechanical Engineering

ABSTRACT

Car air conditioning systems cool the entire cabin, which is inefficient, as only the air surrounding the passengers needs to be cooled to realize a similar effect. These air conditioning units draw large amounts of power, enough to be detrimental to fuel efficiency. This presents problems for cars with smaller engines and electric cars that lack the battery capacity to provide adequate cooling with traditional air conditioning technology. A novel solution to these problems uses evaporative cooling via jumping droplet condensation on superhydrophobic surfaces to provide localized cooling with 100 times less power input. Jumping droplet condensation takes place when microscale droplets coalesce on superhydrophobic surfaces and excess surface energy is converted to kinetic energy, resulting in droplets that jump perpendicularly off the surface. As these droplets fall through the air, they evaporate, cooling the surrounding air and providing localized cooling. To test this technology, a prototype device was designed, fabricated, and tested at different relative humidities in an environmental chamber. Cooling of up to 4.8°C relative to ambient was achieved at 80% relative humidity, 4 cm from the condensing surface. This result suggests an optimal humidity for the operation of these devices and prompts further lines of study for the optimization of this technology.

Thesis Supervisor: Evelyn N. Wang

Title: Associate Professor of Mechanical Engineering

Acknowledgements

I would like to express my sincere gratitude to my thesis advisor, Professor Wang, and the amazing group of people that she has assembled in the Device Research Lab.

I owe a great deal to Dan Preston, a doctoral student in the Device Research Lab. Dan took me in for a UROP the summer after my sophomore year and has allowed me to work with him ever since. I've learned a great deal from him both about being a great researcher and being a great person.

I would also like to thank David Bierman, Dion Savio Antao, Jean Sack, and Solomon Adera for making me feel so welcome in the Device Research Lab and for helping me with experiments. It has truly been a pleasure to work with all of you during my time here.

Thank you also to Bill Cormier for all your help with the fabrication of my experimental setup.

I gratefully acknowledge funding support from the Office of Naval Research (ONR) with Dr. Mark Spector as program manager

Finally, I would like to thank my family and friends for all their support and encouragement along the way.

Table of Contents

List of Tables and Figures

Introduction

In the dead of summer, air conditioning units can be absolutely essential. One place that people have come to expect air conditioning is in their cars. However, air conditioning units draw large amounts of power, making their operation expensive both in terms of cost and fuel efficiency. Car air conditioning units draw close to three kilowatts of power [1], a very significant amount of power given that smaller cars may only produce on the order of 100 kilowatts. The use of air conditioning units is also very problematic in electric vehicles, which simply do not have enough battery capacity to allow air conditioning levels seen in cars with internal combustion engines.

In thinking about how to solve the problems associated with car air-conditioning systems, it is necessary to consider the volume of air being cooled. Current systems cool the entire cabin, which is inefficient, as only the air surrounding the passengers needs to be cooled to provide comfort. An efficiently designed cooling system could essentially create columns of cooled air that fall down on top of the passenger to provide localized cooling.

As a means to achieve localized cooling, this thesis explores the feasibility of mist cooling via jumping droplet condensation. Jumping droplet condensation takes place when water condenses upon surfaces with nanoscale structures that have been treated with superhydrophobic coatings. When the surface has these qualities, the condensed water resides on the surface as discrete small droplets as opposed to covering the surface with a film of water. When adjacent droplets coalesce, there is a decrease in surface energy from the original two droplets to the single coalesced droplet. The released excess surface energy is converted to kinetic energy and the newly formed droplet is able to jump off the surface due to out-of-plane vibrations.

In this application, the jumping droplets can be leveraged to provide localized cooling. By orienting a surface with the condenser side facing downwards towards a passenger, droplets leaving the surface will fall down towards the passenger. As these droplets fall, they evaporate, cooling the air around them. Because the average droplet size is on the order of 10 microns, droplets evaporate quickly, leaving just cool air to envelop the passengers.

The present work shows that, not only does this technology require far less power than current air conditioning systems; it is also silent and will require no maintenance over the device lifetime. Compressor driven air conditioners have many moving parts and refrigerant lines that need to be recharged over time. These jumping droplet mist coolers, however, have no moving parts and are self cleaning.

This thesis explores the feasibility of these devices and determines if such devices could someday be used in place of current air conditioning units in vehicles and elsewhere.

Background

Jumping Droplet Condensation

There are two typical modes of condensation: filmwise and dropwise. Filmwise condensation, which takes place on hydrophilic surfaces, is the most common mode due to the prevalence of high-surface-energy materials in condenser applications. During filmwise condensation, the condensing liquid forms a continuous film on the surface. Conversely, during dropwise condensation, individual droplets form on the surface. Dropwise condensation provides much higher heat transfer rates than filmwise condensation, as the film that forms during filmwise condensation results in a larger thermal resistance; discrete droplets, however, condense and then shed off the surface, opening up new nucleation sites for other droplets to form and grow. This shedding occurs via gravity, with droplets shedding when they reach a critical size.

A subset of dropwise condensation that exhibits even higher heat transfer rates is jumping droplet condensation. This phenomenon occurs when condensation occurs on superhydrophobic surfaces. As the droplets nucleate and grow with time, adjacent droplets coalesce. When this happens, there is a release of surface energy as volume is conserved but liquid-vapor interfacial area decreases. The excess energy is converted into kinetic energy as the droplet jumps off the surface due to out-of-plane oscillations. The droplets being ejected from the surface further increases the heat transfer rate of this type of condensation since their smaller average size before departure results in lower conduction thermal resistance through the drops themselves [2].

Evaporative Cooling

Evaporative cooling is a cooling technology that has been in use for thousands of years. In this process, water droplets added to air evaporate due to a vapor concentration gradient for relative humidity less than 100% and thereby become cooler. When the droplets become cooler

than the surrounding air, they absorb heat from the air. The heat is absorbed as sensible heat, as its movement changes the temperature of the air, but concentration gradient driven evaporation utilizes the latent heat of the water, as it changes the phase of the liquid water into water vapor. Here, the high latent heat of evaporation of water is an advantage to this cooling method, as small amounts of water are capable of absorbing large amounts of heat from the air, cooling the air substantially.

Evaporative cooling is limited, however, by the relative humidity of the air being used. Because the amount of sensible heat that the air can transfer to the water depends upon the amount of humidity that the air can accept, evaporative cooling systems work best in arid environments.

Literature Review

Jumping Droplet Condensation

This project has been made possible by the discovery of jumping droplet condensation from superhydrophobic nanostructured surfaces [3]. This study demonstrated that "30% higher condensation heat transfer coefficient can be achieved using silanized copper oxide (CuO) superhydrophobic surfaces compared to conventional dropwise condensing copper." It also showed that these superhydrophobic nanostructured surfaces can be fabricated at low cost and are readily scalable for different sizes and geometries.

After the discovery of jumping droplet condensation, other applications were realized, such as jumping-droplet electrostatic energy harvesting, which, based upon an earlier paper that showed that jumping droplets leave the surface charged [4], proposed that jumping droplet condensation could be used to harvest energy from natural condensation events, such as morning dew [5]. The droplet charging phenomenon could be taken advantage of in this application to direct droplets towards passengers.

Evaporative Cooling

This work draws upon the study of evaporative cooling droplet evaporation distances conducted by Barrow and Pope in 2007 [6]. This paper determined the distance and time required to for droplets of different diameters to evaporate when falling under their own weight in different relative humidity. For the purposes of this experiment, this analysis needs to be continued in order to take into account multiple droplets evaporating in close proximity, changing the relative humidity as the droplets fall.

Experiment

Device Design

As this device is intended for use in automobiles, the device was designed to be faithful to the realities of operation in an automobile. A schematic of the device experimental test apparatus is shown in Figure 1.

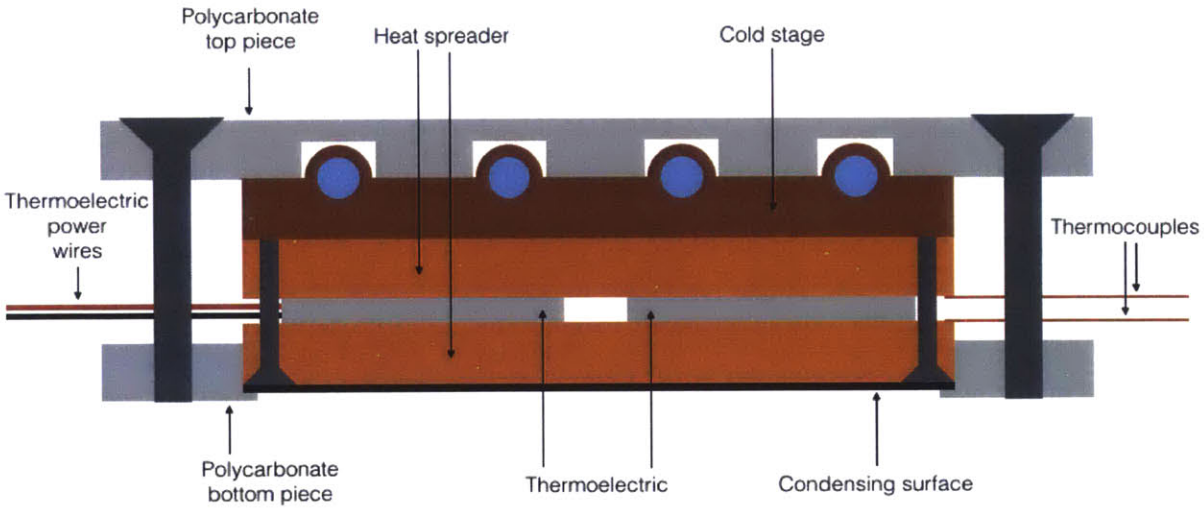

Figure 1. *Schematic of condenser device. The thermoelectric devices are in the middle of the stack as the gray rectangles. These are in thermal contact with a heat spreader on each side. To ensure good thermal contact, the heat spreaders are held together with four 10-32 screws. In contact with the cold side heat spreader is the condensing surface and with the hot side heat spreader is the cold stage. The blue circles in this diagram represent the copper tubing soldered to the cold stage copper block. Water runs through this tubing to remove waste heat from the thermoelectric devices. The entire assembly is held together by two polycarbonate assembly pieces that are also clamped together with nylon screws.*

In order to condense on the superhydrophobic surface, it is necessary to set the temperature of the condenser surface sufficiently low. To establish the necessary temperature difference, thermoelectric devices were chosen because of their ease of use, small size, and lack of moving parts. They are perfect for use in a vehicle, as they rely on electricity to establish a temperature difference and corresponding heat flux. The thermoelectrics chosen for this device

were TE Technology HP-127-1.4-2.5-72. This model was chosen because it offered the lowest heat transfer rate of all of the products in the TE Technology line, which was ideal for this experiment in which high heat fluxes were not needed.

During operation of the thermoelectrics, the heat removed from the condenser surface in addition to the heat created due to thermoelectric inefficiency must be removed from the hot side of the thermoelectric device. In a car, one possible solution to this would be to mount fins on the roof that would reject heat to air moving past the car. In the lab, this potential fin system was simulated with a cold stage comprised of a block of copper with copper tubing soldered into channels milled in the copper block. By running water through the cold stage, heat was removed from the system and a means was provided to set the heat removal rate in order to simulate various fin system conditions. This thermal resistance matching procedure used to set the inlet temperature of the water entering this cold stage and the corresponding MatLab code can be found in the Appendix. The cold stage is shown below in Figure 2.

For the condenser surface, a 100mm x 100mm x 1mm piece of copper was used. This copper sheet was functionalized to become superhydrophobic on one side. The two-step functionalization was performed by growing copper oxide nanoblades on the surface and then coating the surface with a P2i proprietary fluoropolymer coating. This surface displayed an advancing contact angle of 124°±3° and a receding contact angle of 113°±3°, measured with a Kyowa MCA-3 microgoniometer. The surface functionalization process can be found in the Appendix.

Figure 2. *Cold stage used to remove waste heat from thermoelectric devices. The copper block used here is 100 mm x 100 mm x 9.5 mm. The copper tubing is one-quarter inch tubing. To ensure good thermal contact between the block and tubing, a one-quarter inch ball end mill was used to mill four semicircular channels in the block. The tubing was then bent to specifications and soldered into the block.*

Because of the size difference between the four thermoelectrics, which are 40mm by 40 mm, and condensing surface, which was 100 mm by 100 mm, heat spreaders were used to ensure that the entire condenser surface reached the desired temperature. Achieving even cooling across the condenser surface allows the entire surface to be used for condensation. For the heat spreaders, two pieces of 100 mm x 100 mm x 9.5 mm copper were used. These pieces were machined flat on both sides and then lapped to ensure flatness. One of these pieces was tapped with four holes and the other piece was machined with four through holes and countersinking. This was to allow the pieces to be screwed together to sandwich the four thermoelectric devices used. Doing this ensures good thermal contact between the thermoelectrics and the heat spreaders and also makes assembly of the whole device easier. Nylon bolts were chosen because of their low thermal conductivity. Because the bolts were in thermal contact with both the hot and cold sides of the device, it was necessary to reduce the heat transfer back across the temperature difference established by the thermoelectric devices. Using 0.25 W/(mK) as the

thermal conductivity of nylon, the major diameter cross-sectional area of a 10-32 screw, a conduction length of 4.8 mm, and a temperature difference across the thermoelectrics of 39 °C, the heat transfer rate through all four screws was estimated to be 0.149 W, much less than the device cooling rate of 20 W.

It is also necessary to hold the condenser surface onto the cold side heat spreader and the cold stage onto the hot side heat spreader. To do this, two polycarbonate assembly pieces were machined. Polycarbonate was chosen because of its relatively low thermal conductivity of 0.2 W/(mK) in an attempt to insulate the cold stage from the surrounding air. To verify the use of this polycarbonate insulator, the thermal resistance of convection to air calculated using a heat transfer coefficient of 50 W/(m^{2}K) was compared with the thermal resistance of conduction through the polycarbonate. This analysis shows that the polycarbonate insulator conduction resistance is 22.5 times larger than the convection resistance of air, which resulted in significant reduction of parasitic heat loss. The top piece has channels to accommodate the chiller tubes and the bottom piece has a 100mm x 100mm hole to allow the droplets to fall though. This piece also has features to hold the condenser surface in contact with the adjacent heat spreader.

When assembling this device, high silver content thermal grease with a conductivity of 8.85 W/(mK) was used at all interfaces. Estimating the thickness of this grease film to be 50μm and using a heat transfer rate of 20 W, the temperature difference across this interface is estimated to be 0.01 °C. Because this difference is small compared to the other temperature differences in the system, this thermal resistance was neglected.

Experimental Setup

The experimental setup, shown in Figure 3, consists of the condensation device mounted onto an environmental chamber made of 80-20 aluminum extrusion frame and 1/8 inch polycarbonate sheets. This chamber was constructed to allow the device to be tested at different

relative humidities. Images of the experimental setup and condensation device are shown in the Appendix.

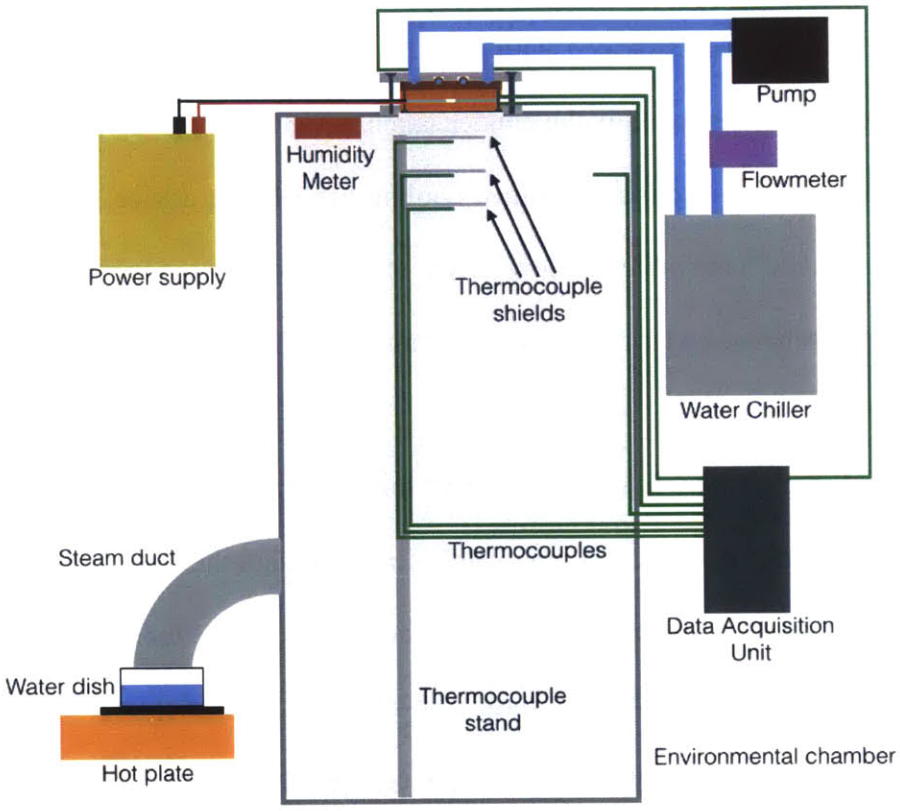

Figure 3. *Schematic of experimental setup for testing condenser device. An image of the setup and device is shown in the Appendix.*

The chamber is four feet tall, two feet wide, and two feet deep. To make the chamber, the 80-20 extrusion was first assembled into the outer dimensions of the box. Then, using 80-20 fasteners, the polycarbonate sheets were attached to the frame. The edges where the 80-20 and polycarbonate interfaced were then sealed with an RTV silicone rubber. A 100 mm x 100 mm opening was cut in the top sheet to allow the condensation device to sit on top and allow droplets to fall into the chamber to achieve localized mist cooling beneath the device. Additionally, one of the side sheets was made removable to allow access to the chamber.

To measure the relative humidity inside the chamber, an Omega RH820U humidity meter was mounted inside the chamber.

To humidify the chamber, a hole was cut in the removable polycarbonate sheet and a piece of flexible aluminum exhaust vent tubing was inserted through this hole and taped in place. The tubing was bent 90 degrees downwards such that the free end of the tubing was parallel with the floor. Directly below this was place a glass dish of water on a hotplate. To increase the humidity in the chamber, the hot plate was turned on and steam was allowed to enter the chamber. When the humidity in the chamber equilibrated at the desired value, the tube was sealed, preventing more steam from entering the chamber.

Once the chamber had reached the desired relative humidity, the chiller loop was turned on to remove waste heat from the thermoelectric devices during operation. The water in this loop was held at constant temperature with a Lauda RE207 thermocirculator. A Cole Parmer 7553-70 MasterFlex peristaltic pump was used to pump the water to the cold stage. To determine the flow rate of water through the cold stage, an Alicat Scientific L-5LPM-D/5V flowmeter was used.

Once the chiller loop was running to remove waste heat, the thermoelectrics were turned on. To power the thermoelectric devices, which were wired in parallel, a Xantrex XHR 60-10 DC power supply was used.

The temperatures at various points in the system were then measured. There were eight Omega J type special limits of error thermocouples in this system, all of which were connected to a Measurement Computing USB-TC data acquisition unit. Figure 3 also demonstrates the thermocouple positions. One thermocouple was inside the chamber, in the top right corner of the chamber to measure the ambient temperature within the chamber. Directly under the condensing surface were three more thermocouples, located 40 mm, 70 mm, and 100 mm from the surface. These thermocouples were mounted to a vertical piece of 80-20 extrusion, labeled in Figure 3 as the "Thermocouple stand." These thermocouples measured any vertical temperature gradient underneath the condensing surface. Three thermocouples were used to determine the temperature gradient as a function of distance from the surface. These three thermocouples had shields above them to prevent droplets jumping off the surface from hitting the thermocouples. Because the condenser surface was held at 3 °C, droplets hitting the thermocouples would give the impression that more cooling is taking place than actually was. These shields were made with copper tape. They can be seen in Figure 4.

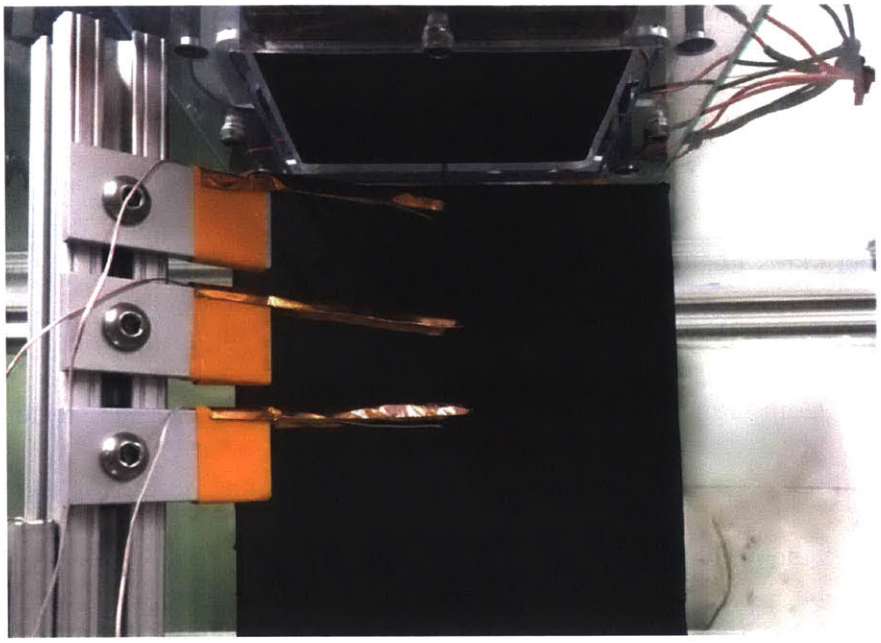

Figure 4. *Thermocouple shields can be seen here. They are the pieces of copper tape extending from the 80/20 extrusion to under the condensing surface. These shields are in place over the thermocouples to prevent jumping droplets from hitting the thermocouples and giving an artificially low thermocouple reading. These shields ensure that the thermocouples are measuring the temperature of the air being cooled by the device.*

There were also two thermocouples fed through Swagelok thermocouple feed-through fittings into the chiller loop flow. These thermocouples measured the temperature of the water immediately before and after it enters the cold stage. This allowed the calculation of the amount of sensible waste heat removed from the thermoelectric devices. Finally, there were two thermocouples dedicated to measuring the temperatures of the hot and cold sides of the thermoelectric devices. By knowing this temperature difference and the voltage across the thermoelectric devices, it is possible to determine the amount of heat being moved by the thermoelectric devices.

To gather data, the following procedure was used. First, the steam duct was opened and the hot plate was turned on. At the same time, the thermocirculator temperature was set, but the peristaltic pump was not turned on. The humidity was then monitored until it hit the desired value. At this point, the steam duct was closed. Then, the peristaltic pump was turned on and set

to the correct flow rate. After verifying that the cold stage inlet temperature was correct, the thermoelectric devices were turned on and the voltage was set to establish a suitable temperature difference while the humidity was monitored to ensure a constant level. Thermocouple data was then collected through LabVIEW 2014.

Thermocouple Calibration Procedure

The type J thermocouples were all calibrated prior to running any experiments. To calibrate them, their ends were submerged in the bath of the Lauda RE207 thermocirculator. The bath temperature was then set to five different temperatures: 5 °C, 10 °C, 15 °C, 20 °C, and 25 °C. At each temperature, the reading of each thermocouple was recorded. Then, for each thermocouple, a linear fit was performed with the measured temperature as the independent variable and the actual bath temperature as the dependent variable. These linear fits were then entered into LabView to correct the measured thermocouple temperature. The results of these linear fits can be seen in Figure 4.

Thermocouple	Linear Fit
1	T_actual = 1.0092T_meas - 0.1673
2	T_actual = 1.0031T_meas - 0.0456
3	T_actual = 1.0082T_meas - 0.4019
4	T_actual = 1.0149T_meas+ 0.2443
5	T_actual = 1.0143T_meas + 0.5091
6	T_actual = 1.0121T_meas + 0.2718
7	T_actual = 1.0141T_meas + 0.2152
8	T_actual = 1.0091T_meas - 0.5498

Table 1. *Table of linear fit lines for thermocouple calibration*

Results and Discussion

Testing of this prototype jumping droplet evaporative cooling device revealed that it is capable of providing localized cooling and its performance is a function of relative humidity. A maximum temperature difference of 4.88 °C was measured at 80% relative humidity, 40 mm from the condensing surface. A similar temperature difference was measured at 70% relative humidity, 40 mm from the condensing surface. It must be noted that when the device was run at the lowest relative humidity, there was a 1.66 °C temperature difference between the ambient and 40 mm thermocouple. This could be due to convective cooling due to the proximity to the surface. However, because the condensing surface was kept at 3 °C for all tests, the temperature difference significantly increases with relative humidity and has a maximum point, as expected, it is very likely that evaporative cooling from jumping droplet condensation was responsible for the cooling performance. The temperature difference as a function of relative humidity in the chamber is shown in Figure 5. Figure 6 shows the mean temperature as a function of relative humidity.

The maxima between 70% and 80% relative humidity suggests that there exists an ideal relative humidity for jumping droplet evaporative cooling. This likely has to do with interplay between high relative humidity increasing the rate of condensation and therefore jumping and low humidity being more favorable to evaporation and therefore cooling. Because jumping occurs as droplets coalesce, high condensation rates are necessary to sustain high rates of jumping droplets. In order to sustain high condensation rates, high humidity is required.

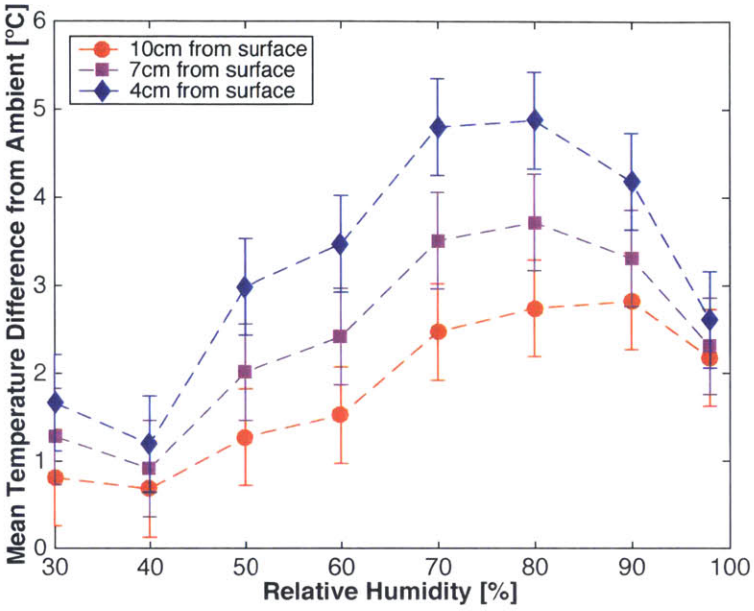

Figure 5. *Temperature difference between ambient and three distances from the condensing surface. There is a maximum temperature difference that occurs around 70-80% relative humidity and 40 mm from the condensing surface. This temperature difference was measured to be 4.80 °C at 70% relative humidity and 4.88 °C at 80% relative humidity. Temperature difference decreases as the distance from the condensing surface increases. Error bars represent Omega J-type thermocouple special limits of error of 1.1 °C.*

However, at high humidities, because the air has a large amount of water vapor in it, droplets are not able to evaporate as easily. When the droplets are unable to evaporate, they cannot cool the air, as cooling takes place when heat moves from the air into the water to evaporate it.

For all humidities tested, the temperature difference decreased with distance from the condensing surface. To explain this, the Barrow and Pope paper can be helpful. In his doctoral thesis, N. Miljkovic determined the distribution of droplet diameters when condensing saturated water vapor on silanized copper oxide (CuO) nanostructures and determined that the roughly 90% of droplets had a diameter of less than 10 μm [7]. This is shown in Figure 7 below, copyright N. Miljkovic, 2013.

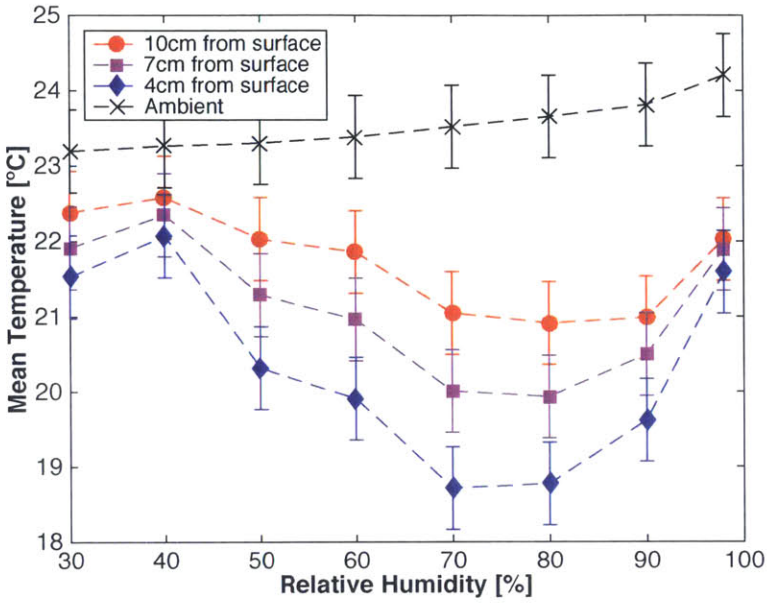

Figure 6. *Temperature at 40 mm, 70 mm, and 100mm below the condensing surface as a function of relative humidity. As can be seen, there is a minimum temperature between 70% and 80% relative humidity. The ambient temperature increased with relative humidity because the air introduced into the chamber to increase the humidity was warmer than ambient. Error bars represent Omega J-type thermocouple special limits of error of 1.1 °C*

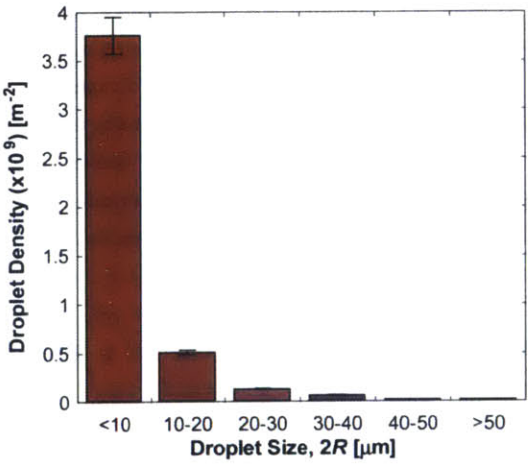

Figure 7. *Distribution of droplet diameters when condensing saturated water vapor on silanized CuO nanostructures. Roughly 90% of droplets had a diameter of less than 10 μm. Because the surface used in this experiment has a more hydrophobic coating and was applied with CVD by P2i, it is expected that the percentage of droplets less than 10 μm in diameter is even higher. This figure is copyright N. Miljkovic, 2013.*

In their paper, Barrow and Pope calculated that droplets with a diameter of less than 25 μm in 40% relative humidity evaporate in 6mm (Barrow and Pope, 2007). This paper used the assumption that the droplets fall under their own weight with no initial velocity, so distances must be adjusted for this experiment, in which the droplets leave the surface with an initial velocity due to the jumping phenomenon. The Barrow and Pope study provides an estimate for droplet evaporation distances, even though the relative humidities were varied in this experiment. Because the P2i surface used in this experiment is more hydrophobic and higher quality, on account of being applied via CVD, it is likely that for this experiment, an even higher percentage of droplets were less than 10 μm in diameter. It is likely that almost all droplets jumping off the surface evaporated and therefore did all their cooling within the first 10 mm of departure from the surface. This means that by the time air reached the thermocouple at 100 mm, it was being warmed by convection and mixing with adjacent air for roughly 10 times long as it was cooled. Based on this, the best way to extend the cooling range is to tune the surface to produce larger droplets that take longer to evaporate. Using the Barrow and Pope model as a starting point and modifying it to account for the effects of surrounding falling droplets to determine the necessary evaporative range, the required droplet size can be estimated in order to design the surface.

For these tests, the thermoelectric devices were run at 6.5 V, drawing 4.4 A of current. This resulted in a temperature difference of 36 °C across the thermoelectrics. From the thermoelectric device data sheets, the device has 20 W of cooling power, but draws 28.6 W, giving a coefficient of performance of 0.69. This is far worse than the COP of compressor driven air conditioners, which are around 3. Despite this fact, this prototype evaporative cooling device is still more efficient, as it uses roughly 100 times less energy than an air conditioner.

This system does take time to reach a steady state cooling, due to fact that the thermoelectric devices must establish a temperature difference before condensation can start and droplets must then nucleate and grow before coalescence and jumping. The start up time of the device in 60% relative humidity is shown in Figure 6.

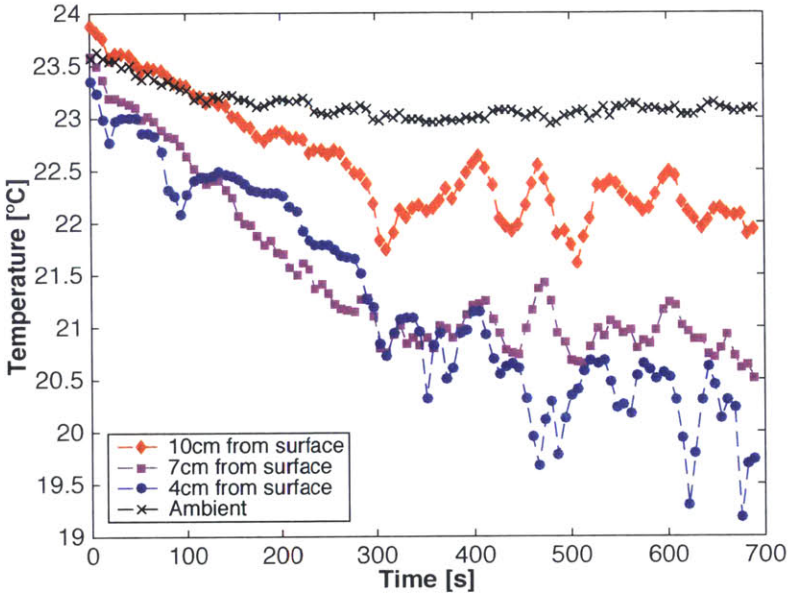

Figure 8. *Temperature in the chamber as a function of time in 60% relative humidity. Time zero corresponds with the thermoelectric devices being turned on. The delay in cooling is due to the fact that the thermoelectric devices need time remove heat from the cold side to establish the prescribed temperature difference. This delay will decrease with decreasing thermoelectric temperature difference.*

This figure also demonstrates the temperature fluctuations that take place with this device. The mechanism behind these fluctuations is not understood, but it could have to do with airflow patterns created by localized cooling of small pockets under the device. These pockets of air could create currents that bring warm air that then takes time to cool off as droplets pass through it.

Conclusion

For the first time, localized evaporative cooling via jumping droplet condensation has been demonstrated. It has been shown that there exists an optimal relative humidity and that the cooling effect is more pronounced closer to the condensing surface of the device.

Both of these findings represent problems for this technology if it is ever to become a viable cooling system for vehicles. Determining the optimal relative humidity is helpful in understanding the dynamics of the system, but for these devices to be integrated into cars, they need to be able to function well at a larger range of humidities. One potential solution to this problem for low relative humidities would be to design the device to introduce high humidity air directly to the condensing surface by boiling water and releasing the humidified air through nozzles close to the surface of the device. This would allow it to sustain high condensation and therefore jumping rates while taking advantage of the low relative humidity in the rest of the vehicle to promote evaporation. However, this would result in a required fluid reservoir that would need to be filled which was not needed in the prototype design.

Additionally, the range of cooling needs to be increased. As mentioned before, this likely requires tuning the condensing surface to produce droplets that jump at a larger diameter than the surface used in this study did. Further research needs to be done to explore surface structures and chemistries that could achieve longer ranged cooling.

Even given these two specific issues with the technology, it is still an exciting alternative to pursue as an alternative to compressor driven air conditioning units. With further optimization and study, localized evaporative cooling via jumping condensation could conceivably find a way into cars around the world.

Bibliography

[1] R. Farrington and J. Rugh, "Impact of Vehicle Air-Conditioning on Fuel Economy, Tailpipe Emissions, and Electric Vehicle Range," *Fuel*, no. September, p. http://www.nrel.gov/docs/fy00osti/28960.pdf, 2000.

[2] N. Miljkovic and E. N. Wang, "Condensation heat transfer on superhydrophobic surfaces," *MRS Bull.*, vol. 38, no. 05, pp. 397–406, 2013.

[3] N. Miljkovic, R. Enright, Y. Nam, K. Lopez, N. Dou, J. Sack, and E. N. Wang, "Jumping-droplet-enhanced condensation on scalable superhydrophobic nanostructured surfaces," *Nano Lett.*, vol. 13, no. 1, pp. 179–187, 2013.

[4] N. Miljkovic, D. J. Preston, R. Enright, and E. N. Wang, "Electrostatic charging of jumping droplets.," *Nat. Commun.*, vol. 4, p. 2517, 2013.

[5] N. Miljkovic, D. J. Preston, R. Enright, and E. N. Wang, "Jumping-droplet electrostatic energy harvesting," *Appl. Phys. Lett.*, vol. 105, no. 1, p. 013111, 2014.

[6] H. Barrow and C. W. Pope, "Droplet evaporation with reference to the effectiveness of water-mist cooling," *Appl. Energy*, vol. 84, no. 4, pp. 404–412, 2007.

[7] N. Miljkovic, "Development and Characterization of Micro / Nano structured Surfaces for Enhanced Condensation," Massachusetts Institute of Technology, 2013.

Appendix A: Chiller Loop Inlet Temperature Calculation

This MatLab code was used in the design of the cold stage to set the cold stage parameters of flow rate and inlet water temperature in order to accurately simulate using a fin system to remove waste heat from the thermoelectric devices.

It is important that both systems have equal heat removal capacities given the temperature differences. It is also important that the hot side thermoelectric temperature be the same in both systems, as the thermoelectric works by establishing a temperature difference. By setting the thermocirculator temperature too low and therefore making the heat removal rate too high, the thermoelectric devices will need to establish a lower temperature difference. This will require less power and give an artificially high thermoelectric efficiency. Although maximizing thermoelectric efficiency was not a goal of this thesis, it is still important to make every effort to faithfully simulate the real use case.

To accurately simulate this system, it was necessary to model a fin system and determine an equivalent thermal resistance for this setup. Then, using the Gnielinski Correlation, a similar calculation was done for a turbulent fluid flow in a pipe.

First, a reasonable fin size was estimated for the roof of a car. The dimensions of this fin are shown in Figure 12.

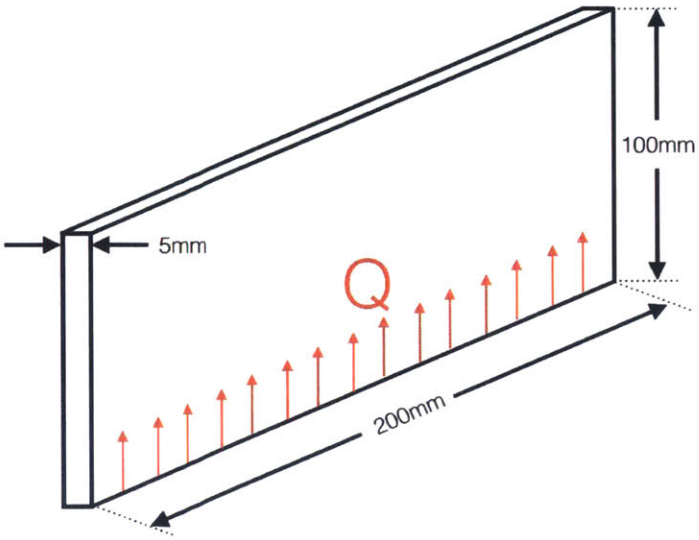

Figure 9. *Dimensions of theoretical fin used to remove heat from thermoelectric devices when condensing device is used in cars. Q denotes the direction that heat travels from the base to the tip.*

Using this fin, the following parameters were calculated:

$$m = \sqrt{\frac{h_{air}P_{fin}}{k_{fin}A_{cross-section}}} \tag{1}$$

$$M = \sqrt{h_{air}P_{fin}k_{fin}A_{cross-section}}\,\Theta_{\boldsymbol{b}} \tag{2}$$

Where $\Theta_{\boldsymbol{b}} = \boldsymbol{T_{base}} - \boldsymbol{T}_{\infty} = \boldsymbol{\Delta T_{fin}}$. The general fin equation was used to model the fin. For this fin, the heat transfer rate is equal to:

$$\dot{Q} = M\frac{\sinh mL + \frac{h}{mk}\cosh mL}{\cosh mL + \frac{h}{mk}\sinh mL} \tag{3}$$

Where L is the length of the fin, h is the heat transfer coefficient of air, and k is the thermal conductivity of the fin.

To make the analysis easier, all equations that solve for $\dot{Q}$ will be considered to be in the form

$$\dot{Q} = U_{equiv}A\Delta T = \frac{1}{R}\Delta T \tag{4}$$

Using this form, and noting that

$$M = \sqrt{h_{air}P_{fin}k_{fin}A_{cross-section}}\,\Theta_{\boldsymbol{b}} = \sqrt{h_{air}P_{fin}k_{fin}A_{cross-section}}\,\boldsymbol{\Delta T_{fin}} \tag{5}$$

We can write R_{fin} as

$$R_{fin} = \frac{\cosh mL + \frac{h}{mk}\sinh mL}{\sinh mL + \frac{h}{mk}\cosh mL}\left(h_{air}P_{fin}k_{fin}A_{cross-section}\right)^{-\frac{1}{2}} \tag{6}$$

Although the contribution is small from convection from the flat areas at the base of the fins, it will be considered here.

The thermal resistance of these areas will be equal to

$$R_{flat} = \frac{1}{h_{air}A_{flat}} \tag{7}$$

The resistance through the roof will be equal to

$$R_{roof} = \frac{t_{roof}}{k_{roof}A_{device}} \tag{8}$$

The total resistance for the fin system will be

$$R_{total,fin} = \left(\frac{n_{fins}}{R_{fin}} + \frac{1}{R_{flat}}\right)^{-1} + R_{roof} \tag{9}$$

We can now consider the thermal resistance of the cold stage and chiller loop. Using the Churchill equation for the friction factor within the tube, we find that f is equal to

$$A_1 = \left(2.457 \ln\left(\left(\left(\frac{7}{Re}\right)^{0.9} + 0.27\frac{\varepsilon}{D}\right)^{-1}\right)\right)^{16} \tag{10}$$

$$A_2 = \left(\frac{37530}{\mathrm{Re}}\right)^{16} \tag{11}$$

$$f = 8\left(\left(\frac{8}{Re}\right)^{12} + (A_1 + A_2)^{-1.5}\right)^{\frac{1}{12}} \tag{12}$$

Then, the Gnielinski Correlation can be used to calculate the Nusselt number inside the tube for the turbulent flow.

$$Nu_D = \frac{(f/8)(\mathrm{Re} - 1000)\mathrm{Pr}}{1 + 12.7(f/8)^{1/2}(\mathrm{Pr}^{2/3} - 1)} \tag{13}$$

Then,

$$h_{tube} = \frac{k_{water}}{D} Nu_D \tag{14}$$

The resistance due to convection will be

$$R_{tube,conv} = \frac{1}{h_{tube}A_{tube,surface}} \tag{15}$$

The resistance through the tubing will be

$$R_{tube,cond} = \frac{\ln\frac{D_{outer}}{D_{inner}}}{2\pi l_{tube}k_{tube}} \tag{16}$$

The resistance through the base of the cold stage is

$$R_{base} = \frac{t_{base}}{k_{base}A_{base}} \tag{17}$$

Therefore, the total resistance for the cold stage, as all resistances are in series is,

$$R_{base} = R_{tube,conv} + R_{tube,cond} + R_{base} \tag{18}$$

We can now equate the heat transfer rates for the two cooling systems. We must also be careful that the hot side temperatures are the same for both cases.

$$\dot{Q}_{fin} = \dot{Q}_{chiller} \tag{17}$$

$$\frac{1}{R_{fin}}(T_{hot} - T_{\infty}) = \frac{1}{R_{chiller}}(T_{hot} - T_{chiller,in}) \quad (18)$$

We can then manipulate this equation to determine the inlet water temperature for the chiller.

$$T_{chiller,in} = T_{hot} - \frac{R_{chiller}}{R_{fin}}(T_{hot} - T_{\infty}) \quad (19)$$

With this equation, we can determine the correct inlet temperature given the target hot side temperature and the ambient temperature for the fin system. The hot side temperature will be determined by the desired condensing surface temperature, thermoelectric temperature difference, and heat removal rate.

```
%% Chiller Loop Inlet Water Temperature Calculation
%% John Queeney
%% April 24, 2015

%% Fin Thermal Resistance
T_amb = 25;     %[C]
n_fins = 10;    %[]

k_Al = 237;     %[W/mK] aluminum thermal conductivity
k_Cu = 401;     %[W/mK] copper thermal conductivity

%Geometry
h_air = 50;    %[W/m^2K]
k_fin = k_Al; %Aluminum fins
t_fin = .005; %[m]
w_fin = 0.2;  %[m]
l_fin = 0.1;  %[m]
A_base = .1^2;%[m^2]
A_between_fins = A_base-t_fin*w_fin*n_fins;

k_roof = 200;  %[W/m^2K]
t_roof = 0.001;%[m]

A_c_fin = t_fin*w_fin;    %Cross Sectional Area of fin
P_fin = 2*t_fin+2*w_fin; %Perimeter of fin

%Adiabatic Tip Fin
m_fin = sqrt((h_air*P_fin)/(k_fin*A_c_fin));
%M with Theta_b divided out
M_fin_prime = sqrt(h_air*P_fin*k_fin*A_c_fin);

R_fin =
(M_fin_prime*((sinh(m_fin*l_fin)+(h_air/(m_fin*k_fin))*cosh(m_fin*l_fin))/...
(cosh(m_fin*l_fin)+(h_air/(m_fin*k_fin))*sinh(m_fin*l_fin))))^-1;

R_area_between_fins = 1/(h_air*A_between_fins);

R_roof = t_roof/(k_roof*A_base);

R_fin_side_total = (n_fins/R_fin + 1/R_area_between_fins)^-1 + R_roof;

UA_fin_total = R_fin_side_total^-1;
```

```
%% Chiller Loop Thermal Resistance

%Geometry
OD_tube = 6.35/1000; % [m] tube outer diameter (0.25 inch tube)
ID_tube = 4.19/1000; % [m] tube inner diameter
l_tube = 640/1000;   % [m] tube length

SurfaceArea_outside_tube = pi*OD_tube*l_tube; %[m^2]; total tube condensing
surface area
A_cross_section_tube = (pi*ID_tube^2)/4;      %[m^2]; tube inner cross-
sectional area
SurfaceArea_inside_tube = pi*ID_tube*l_tube;  %[m^2]; tube inner surface area

t_baseplate = .25*2.54/100; % [m]
A_baseplate = .1^2;         % [m^2]

k_tube = k_Cu;

eps_Cu = 0.0000015;         %surface roughness [m] copper pipe
eps_smooth = 0;

eps = eps_smooth;

% Fluid Properties
T_coolant = 36.5;                                   %[C]

%liquid water heat capacity inside tube
C_p_water = XSteam('CpL_T',T_coolant)*1000;         %[J/kgK]

%liquid water thermal conductivity inside tube
k_water = XSteam('tcL_T',T_coolant);                %[W/mK]

%liquid water density
rho_water = XSteam('rhoL_T',T_coolant);             %[kg/m^3]

%liquid water dynamic viscosity
mu_water = XSteam('my_pT',1,T_coolant);             %[Pa s]
mu=mu_water;

% cooling water Prandtl number
Pr = C_p_water*mu_water/k_water;                    %[]

% Friction factor
% enter this flow rate as  LPM*(1.67*10E-5)
vol_flow_rate = 0.6*((5/3)*1E-5);                   %[m3/s]

%cooling water flow velocity
v_water = vol_flow_rate/A_cross_section_tube;       %[m/s]

% cooling water flow Reynolds number
Re = rho_water*v_water*ID_tube/mu;                  %[]

% cooling water friction factor (Churchill - accounts for laminar)
A1 = (-2.457*log((7/Re)^0.9+0.27*eps/ID_tube))^16;
A2 = (37530/Re)^16;
```

```
f_c = 8*[(8/Re)^12+1/(A1+A2)^1.5]^(1/12);

f = f_c;

% Condensation Heat Transfer Coefficient (Gnielinski)
Nu_inside_tube = ((f/8)*(Re-1000)*Pr)/(1+12.7*(f/8)^(1/2)*(Pr^(2/3)-1));

h_inside_tube = (k_water/ID_tube)*Nu_inside_tube;   % [W/m^2K]; cooling water
heat transfer coefficient - Gnielinski

R_inside_tube = 1/(h_inside_tube*SurfaceArea_inside_tube);

R_tube = log(OD_tube/ID_tube)/(2*pi*l_tube*k_tube);

R_baseplate = t_baseplate/(k_Cu*A_baseplate);

R_chiller_side_total = R_inside_tube+R_tube+R_baseplate;

UA_chiller_side = R_chiller_side_total^-1;

%% Thermoelectric Performance

cooling_capacity = 500; %[W/m2] Cooling capacity specified in proposal

Q_device_min = cooling_capacity*A_base;  %[W]

Q_removed_per_TE = 5;

num_TE = 4;

Q_removed_total = num_TE*Q_removed_per_TE;

% TE performance data from TE Technology Datasheet for Potted
% HP-127-1.4-2.5-72 with hot-side temp of 50C

% We want Q_dot to be equal for chiller and fin situations
% UA_fin * (T_base - T_amb) = UA_chiller * (T_base - T_water)
% We also want T_base to be identical. T_base here is 50C
% We need to determine what the input temperature of the chiller water
% should be.
% This gives us:

T_base = 40;

T_air = 35;

T_chiller_water_in = T_base - (UA_fin_total/UA_chiller_side)*(T_base-T_air)

Q_waste_heat = 11;                          %[W]

vol_flow_rate = 0.6*((5/3)*1E-5);           %[m3/s] enter this flow rate as
LPM*(1.67*10E-5)

dT_COOLANT = (Q_waste_heat*num_TE)/(vol_flow_rate*C_p_water*rho_water)
```

Appendix B: Copper Oxide Nanostructure Integration Procedure

Type I CuO Integration Procedure
Procedure by Youngsuk Nam, written by Nicholas Dou

Materials
All equipment specifically for this procedure has a blue label.

Tweezers	Sonicator	DI water
Spoons (2)	Scale	Solvents (acetone, methanol, IPA)
Beaker	Hot plate with stirring	HCl (2 M)
Graduated cylinder	Thermometer	$NaClO_2$
Weighing paper		NaOH
Glass dish		$Na_3PO_4 \cdot 12H_2O$
Glass cover		Air (N_2)
Teflon cover		

Solution preparation

1. Prepare solution in dish

DI water	100 mL	150 mL		**300mL**
Sodium chlorite ($NaClO_2$)	3.75 g	5.625 g	**Increase 25%**	**14.063g**
Sodium hydroxide (NaOH)	5 g	7.5 g		**15g**
Trisodium phosphate dodecahydrate ($Na_3PO_4 \cdot 12H_2O$)	10 g	15 g	**Decrease 25%**	**22.5g**

   Quantities can be scaled
   Greater volume → less thermal fluctuation (more mass), less uncertainty in mixture quantities
   Sodium chlorite is the strongest and most hazardous; use a separate spoon
   Err on the side of more, so the solution will be stronger
2. Heat/stir solution to 95°C
   Settings: ~230 °C, stirring on (any speed)
   Takes some time, clean samples while waiting

Cleaning
1. Use solvents to remove organic contaminants
   a. Sonicate with samples in a small beaker with acetone (sonication bath is filled with DI water)
   b. Rinse with methanol, IPA, water (in that order)
   c. Dry with N_2 or Air in fume hood (orange valve)
2. Use HCl to remove existing oxide
   a. Dip in 2 M solution for ~30 seconds—To make more, add 33.4ml 12M HCl to 200ml water
   b. Rinse with water
   c. Dry

Samples should become visibly lighter in color

Integration of structures

3. Add clean copper samples
4. Maintain temperature at 95 °C for 5 minutes.
   Settings: ~180 °C, no stirring
   Samples should turn black
   Timing is not critical; structures will be stable after a certain time.
5. Remove, rinse, and dry samples
   Solution will leave residue if not cleaned immediately!
6. Safely dispose the solution
7. Rinse and clean dish immediately afterwards
   Solution will leave residue if not cleaned immediately!
8. Dry on hotplate at 80C for at least 1 hour
9. Clean all other equipment

Appendix C: Images of Experimental Setup and Device

Figure 10. *Image of experimental setup. The thermocirculator is missing from this image.*

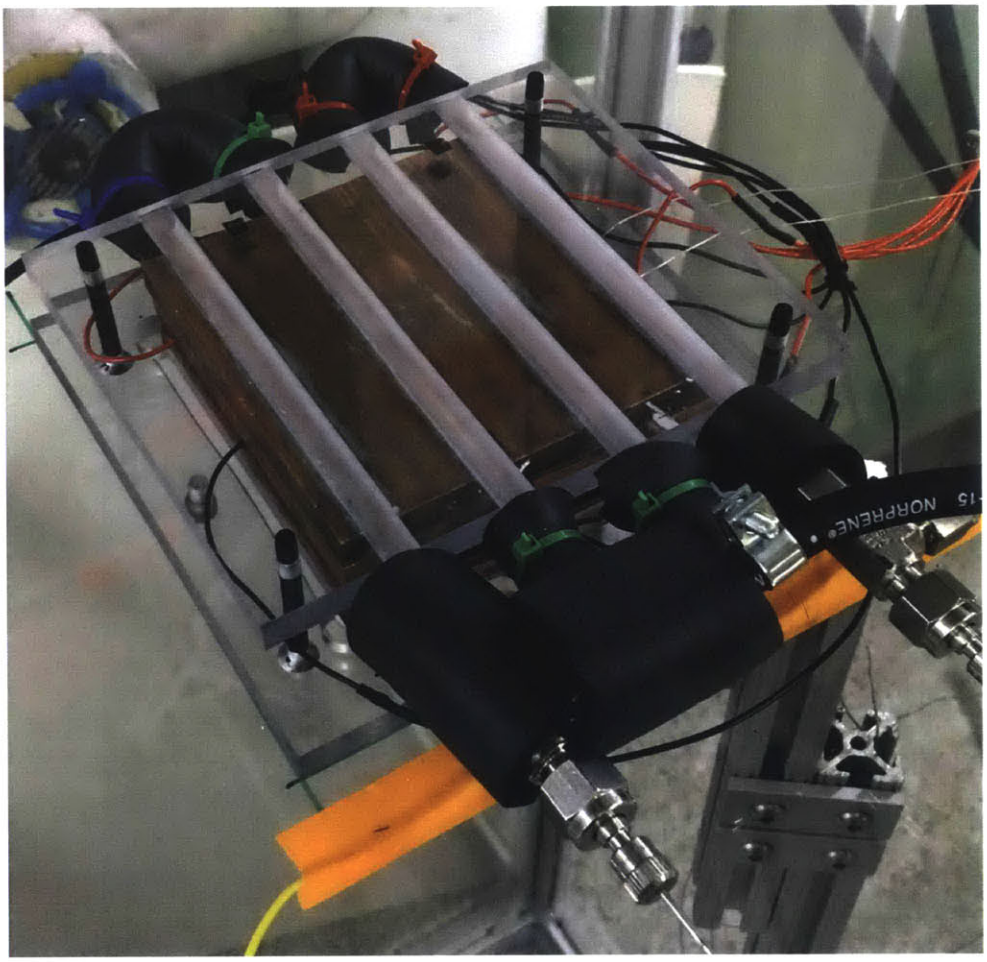

Figure 11. *Image of condensation device mounted on environmental chamber for testing. Insulation was added around the copper tubing where it protruded from the polycarbonate to reduce heat transfer to the water from the environment.*